Osteoclast-mediated acidic hydrolysis of thermally gelled curdlan component of the bone scaffolds: Is it possible?

Agata Przekora [a,*], Letizia Penolazzi [b], Grzegorz Kalisz [c], Paulina Kazimierczak [a], Cristina Canal [d,e,f], Michal Wojcik [a], Roberta Piva [b], Anna Sroka-Bartnicka [c]

[a] Independent Unit of Tissue Engineering and Regenerative Medicine, Medical University of Lublin, Chodzki 1 Street, 20-093 Lublin, Poland
[b] Department of Neuroscience and Rehabilitation, University of Ferrara, via Fossato di Mortara 74, 44121 Ferrara, Italy
[c] Independent Unit of Spectroscopy and Chemical Imaging, Medical University of Lublin, Chodzki 4a Street, 20-093 Lublin, Poland
[d] Biomaterials, Biomechanics and Tissue Engineering Group, Materials Science and Engineering Department, Research Center for Biomedical Engineering, Technical University of Catalonia (UPC), Escola d'Enginyeria Barcelona Est (EEBE), C/Eduard Maristany 14, 08019 Barcelona, Spain
[e] Barcelona Research Center in Multiscale Science and Engineering, UPC, 08019 Barcelona, Spain
[f] Institut de Recerca Sant Joan de Déu, Santa Rosa 39-57, 08950 Esplugues de Llobregat, Spain

ARTICLE INFO

ABSTRACT

Many biomaterials for bone regeneration have recently been produced using thermally gelled curdlan (1,3-β-D-glucan) as a binder for bioceramics. As the human organism does not produce enzymes having the ability to degrade curdlan, it is not clear what is the fate of curdlan gel after its implantation in the bone. To clarify this point, in this research osteoclasts were cultured on the curdlan gel to show its degradation by acidic hydrolysis. The studies clearly demonstrated microstructural (AFM and SEM imaging) and chemical changes (Raman spectroscopy) on the curdlan surface caused by osteoclast culture. Moreover, degradation test in a cell-free system using HCl solution (pH = 4.5), mimicking environment in the resorption lacuna, showed great weight loss of the sample, release of glucose, and chemical changes typical of curdlan degradation. Thus, the presented research for the first time provides a strong evidence of osteoclast-mediated acidic hydrolysis of thermally obtained curdlan gel.

1. Introduction

Curdlan, a linear 1,3-β-D-glucan, is an exopolysaccharide characterized by high molecular weight which is between 2.06×10^4 and 5.0×10^6 Da (Chaudhari et al., 2021). This homopolymer of D-glucose connected by β-1,3-glycosidic bonds was isolated for the first time in 1962 from *Alcaligenes faecalis* var. *myxogenes* 10C3 (Aquinas et al., 2021). Nowadays it is known that curdlan may be obtained by microbial synthesis using various soil bacteria belonging to species of Genus *Alcaligenes*, *Agrobacterium*, *Rhizobium*, *Bacillus*, and *Cellulomonas* (Martinez et al., 2015). Among them, the non-pathogenic *Agrobacterium* sp., a gram-negative bacterium, is the most frequently used for curdlan synthesis (Aquinas et al., 2021). *Agrobacterium fabrum*, commonly known curdlan-producing strain, was isolated from the nodules of groundnut and pea plant (Laxmi et al., 2018). On an industrial scale, curdlan is produced by using two bacterial strains that are commercially available in American Type Culture Collection (ATCC): *Agrobacterium* sp. ATCC 31749 and *Agrobacterium* sp. ATCC 31750 (Chaudhari et al., 2021; Yu et al., 2015).

Curdlan possesses some important features that make this polysaccharide a promising candidate to be used in a multitude of applications. It was proven to be biodegradable, non-toxic to eukaryotic cells and the environment, and to have the ability to form stable gels by heating of aqueous curdlan suspension or dialysis of alkaline curdlan solution against calcium salt (Klimek et al., 2017; Zhang & Edgar, 2014). Importantly, curdlan was approved by the U.S. Food and Drug Administration (FDA) in 1996 (Mangolim et al., 2017). So far, it was used in food industry as water-holding agent or as a stabilizer of physical properties of some products, e.g. fish pastes and noodles (Chaudhari et al., 2021; Przekora & Ginalska, 2014). Recently, a growing interest in the biomedical and pharmaceutical applications of curdlan is observed. Curdlan was used as effective drug carriers (Tukulula et al., 2015), antibacterial curdlan/chitosan blending membranes (Sun et al., 2011), wound dressings (Michalicha et al., 2021; Wojcik, Kazimierczak, Benko,

et al., 2021; Wojcik, Kazimierczak, Vivcharenko, Koziol, & Przekora, 2021), and bone scaffolds/implants for regenerative medicine applications (Borkowski et al., 2021; Klimek et al., 2017; Przekora & Ginalska, 2014, 2016).

In the case of scaffolds for bone regeneration, it is important that the biomaterial is bioabsorbable, allowing for good osseointegration and gradual replacement of the implant by newly-formed bone (Przekora, 2019). Bioabsorbability is the process by which the bone implant is absorbed in the body after implantation, either by cells (osteoclast-mediated resorption), dissolution or biodegradation. As bone tissue consists of an organic matrix and a mineral part consisting of hydroxyapatite (HA), a vast majority of bone scaffolds is made of calcium phosphate ceramics such as HA or α-/β-tricalcium phosphate (TCP), and other components in the form of biopolymers (e.g. collagen, alginate, amylopectin, chondroitin sulphate, chitosan) or synthetic polymers (e.g. poly(glycolic acid) (PGA), polylactic acid (PLA)) which mimic the organic part of the bone tissue (Przekora, 2019; Przekora & Ginalska, 2014). While calcium phosphate ceramics are known to be resorbed by osteoclasts during the bone remodeling process (Diez-Escudero et al., 2017, 2019), degradation of polymer matrix of novel biomaterials must be experimentally investigated. Some of the polymers, which are commonly used for bone scaffold fabrication, were proven to be degraded via either enzymatic (e.g. chitosan, collagen) or hydrolytic (e. g. PGA, PLA) mechanism (Leong et al., 2008).

Since curdlan is non-toxic and has the unique ability to form stable gel after heating its aqueous suspension, many biomaterials for bone regeneration have been recently produced using this polysaccharide as a binder for calcium phosphate ceramics. Osteoclasts produce proteolytic enzymes that degrade the bone extracellular matrix (ECM) and some polymer components of the biomaterials (Everts et al., 2006), whereas bone mineral and bioceramics components are dissolved by acidification occurring in the resorption lacuna (Henriksen et al., 2008; Low & Kopeček, 2012). However, human organism does not produce enzymes capable of curdlan degradation, thus curdlan belongs to the polymers with unknown degradation mechanism after implantation within the bone *in vivo* and its fate in the living organism is unidentified. Therefore, it is not clear whether curdlan-based bone implants may be fully replaced with newly formed tissue. Importantly, this bacterial 1,3-β-D-glucan was proven to be degraded only by some glucanase and glucosidase enzymes produced by fungi, yeast or bacteria. It may also undergo degradation via acidic hydrolysis, usually at high temperature of 80–100 °C (Gidley & Nishinari, 2009; Zhang & Edgar, 2014). Although curdlan solution was proven to undergo acidic hydrolysis, thermally gelled curdlan (obtained from its water suspension) was demonstrated to be quite resistant to acidic hydrolysis (Gidley & Nishinari, 2009).

Taking into account that the human organism does not produce appropriate enzymes required for degradation of the curdlan matrix after its implantation, it is very important to determine degradation mechanism of thermally gelled curdlan, which is the component of many bone scaffolds. As osteoclasts degrade bone by secretion of proteolytic enzymes (Everts et al., 2006) and primarily by acidification of the surrounding environment (Henriksen et al., 2008; Low & Kopeček, 2012), it was hypothesized that curdlan gel may undergo osteoclast-mediated degradation via acidic hydrolysis due to significantly lowered pH (4.0–4.5) in the resorption lacuna. To test our hypothesis, we conducted comprehensive degradation studies on the thermally gelled curdlan matrix with the use of osteoclast culture and advanced spectroscopic and microscopy methods (e.g. Raman spectroscopy, AFM, CLSM, SEM). Considering that not only osteoclasts produce reactive oxygen species (ROS) and reactive nitrogen species (RNS) during bone resorption, but also biomaterial may activate immune cells to produce elevated ROS/RNS leading to oxidative damage of the implant, potential ROS/RNS-mediated degradation of the curdlan gel was also determined. This approach allowed to get an answer to the persistent question whether curdlan gel, which is not prone to enzymatic degradation in the human body, may undergo osteoclast-mediated acidic hydrolysis during

bone resorption process.

2. Materials and methods

2.1. Fabrication of thermally gelled curdlan matrix

The thermally irreversible curdlan gel in the form of a thin matrix was prepared using curdlan powder purchased from Wako Chemicals (Japan). The curdlan (cat. No. 281-80531; DP 6790; molecular formula: $(-C_6H_{10}O_5-)_n$; specific rotation: $[\alpha]_D^{20} = +30° \sim +35°$; gel stability: pH 2.0–9.5 with max. gel strength: pH 2.0–3.0) was produced by microbial synthesis using *Alcaligenes faecalis* var. *myxogenes*. Curdlan suspension (8 % *w/v*) was prepared in a sterile deionized water and then it was spread on the 13 mm diameter round glass coverslip. The thermally gelled curdlan matrix was obtained by 20 min heating in a waterbath at 90 °C. Curdlan samples were air-dried at room temperature and subjected to sterilization using ethylene oxide. The thickness of the dried curdlan matrix was estimated to be 95 μm ± 8.3 μm using electronic micrometer with accuracy 0.001 mm (Schut Geometrical Metrology, Groningen, The Netherlands).

2.2. Osteoclast culture on curdlan gel

Human osteoclasts were prepared as reported by Matsuzaki et al. (1999) with slight modification. Briefly, peripheral blood (PB) was collected from healthy normal volunteers after informed consent. PB mononuclear cells (PBMCs) were prepared from diluted PB (1:2 in Hanks Balanced Salt Solution) which was layered over Histopaque 1077 (Sigma Aldrich-Chemicals, USA) solution, centrifuged (400 *g*), then washed and resuspended in D-Minimum Essential Medium (MEM) (Euroclone, S.p.A., Italy)/10 % FBS (Euroclone, S.p.A., Italy). Curdlan matrices were placed in agarose-coated 24-multiwell plates and preincubated in complete culture medium prior to cell seeding. 1×10^6 PBMCs were seeded on curdlan matrices and allowed to settled for 16 h; wells were then rinsed to remove non-adherent cells. Monocytes were then cultured in Dulbecco's MEM supplemented with 10 % FCS, 100 U/mL penicillin and 10 U/mL streptomycin for 14 days in presence of 25 ng/mL human macrophage colony-stimulating factor (M-CSF) and 30 ng/mL receptor activator for nuclear factor κB ligand (RANKL) (Sigma Aldrich-Chemicals, Poland). Culture media were replenished with fresh media every 3–4 days until osteoclast maturation. Curdlan matrices unseeded with osteoclasts were maintained in the complete medium through the experiment and served as control samples.

2.2.1. Actin belt fluorescent staining

Active osteoclasts on the curdlan matrix were also observed by confocal laser scanning microscope (CLSM, Olympus Fluoview equipped with FV1000, Japan) upon fluorescent staining of actin belt. For this purpose, samples after osteoclasts culture were fixed in 4 % formaldehyde, permeabilized with 0.2 % TritonX-100 (both reagents from Sigma-Aldrich Chemicals, Poland), and stained using AlexaFluor635-Phalloidin (Invitrogen, USA) and DAPI (Sigma-Aldrich Chemicals, Poland) to visualize F-actin filaments and cell nuclei, respectively. The staining procedure was described previously (Vivcharenko et al., 2020). Additionally, vinculin was immunostained using human specific anti-vinculin primary antibody and secondary antibody conjugated to AlexaFluor488 (both antibodies purchased from Abcam, UK). Imunnofluorescent staining was described earlier (Przekora et al., 2017).

2.2.2. TRAP immunohistochemistry staining

To visualize mature osteoclasts, tartrate-resistant acid phosphatase (TRAP) immunohistochemistry staining was performed. Cells were fixed in 3 % para-formaldehyde with 0.1 M cacodilic buffer, pH 7.2 (0.1 M Sodium cacodilate, 0.0025 % CaCl₂) for 15 min, extensively washed in the same buffer, and stained for TRAP (Acid Phosphatase Kit no. 386 – Sigma, St. Louis, MO, USA). After washing with distilled water and

drying, mature TRAP positive multinucleated cells containing more than three nuclei were considered as osteoclasts.

2.3. Analysis of microstructural and chemical changes

The samples after osteoclast culture were subjected to osmotic lysis in distilled water to remove the cells from the surface of the curdlan matrix. Then, the samples were air-dried and analysed using spectroscopic and microscopic techniques. To check whether osmotic lysis was efficient and there were no cellular debris on the surface of curdlan gel that could have affected gel topography, protein staining using 20 ng/mL Texas Red C_2-maleimide dye (Thermo Fisher Scientific, USA) followed by CLSM observation was performed. Obtained CLSM images clearly showed that osmotic lysis was efficient since there were no cellular debris (red fluorescence) on the surface of the curdlan gel (Supplementary Material 1a). Moreover, SEM imaging (conducted as described in Section 2.3.2) carried out for curdlan gel after incubation in distilled water confirmed that osmotic lysis did not affect topography of the sample (Supplementary Material 1b).

2.3.1. Atomic force microscope imaging

Changes in topography of curdlan samples were monitored by AFM (Dimension 3100, Veeco Digital Instruments, Bruker, Germany). Height and amplitude images were recorded simultaneously in tapping mode in air using a silicon Tap150al-G cantilever (NanoWorld Group, Neuchâtel, Switzerland) at a scan rate of 1 Hz. Peak and valley areas of 1×1 μm^2 were analysed for CTR and patterned curdlan surfaces to obtain Sa-nano-peak and Sa-nano-valley, respectively.

2.3.2. SEM imaging

For scanning electron microscope (SEM) imaging, the samples were dehydrated in graded ethanol concentrations of 35 %, 50 %, 75 %, 95 %, and 99.8 % and dried curdlan matrices were sputtered with a 8 nm gold layer. The samples were then observed using SEM (JEOL JCM-6000Plus, Japan) operated in a high vacuum environment at an accelerating voltage of 5 kV.

2.3.3. Raman spectroscopy

Chemical changes on the surface of curdlan gel upon osteoclast culture were analysed by Raman spectroscopy, using a DXR Raman Microscope (Thermo Scientific, USA). The device was equipped with a laser of 780 nm excitation wave and output power of 15 mW. For obtaining the best Raman intensity of recorded spectra, parameters of measurement were optimised in spectral range of 200–3000 cm^{-1} with $10\times$ objective and CCD camera (Sentech, Ebina, Japan) with 0.8-megapixel CCD sensor. A 50-pinhole aperture was used for single spectra recording and mapping. Mapping consisted of 3 μm step size at total area of measurement 0.02 mm^2. Spectra and maps were recorded and the data were analysed with dedicated software (Omnic ver. 8.2.0.387, Thermo Fisher Scientific, USA). Measurements of peak heights were analysed by an unpaired *t*-test to evaluate statistically significant differences ($p < 0.05$) between treated and control samples (Microsoft Excel 2019, ver 2201).

2.4. Degradation test on curdlan matrix in a cell-free system

The test was performed using unseeded curdlan samples and degradation solution (HCl), pH = 4.5 (Avantor Performance Materials, Poland) mimicking conditions occurring in the resorption lacuna during osteoclast-mediated bone resorption. Samples treated with phosphate buffered saline (PBS, Sigma-Aldrich Chemicals, Poland) served as control samples.

2.4.1. Microstructural and chemical changes

The 80 μL droplet of degradation solution (HCl, pH = 4.5) or PBS (control) was placed on the surface of curdlan matrices and the samples were put into the cell culture incubator (37 °C, 5 % CO_2, 95 % humidity) for 14 days. Every 4–5 days (when degradation solution dried out form the surface) another droplet of degradation solution or PBS was placed. After 14 days of incubation, samples were air-dried and subjected to SEM imaging and Raman spectroscopy analysis as described in sections above.

2.4.2. Quantitative analysis of curdlan degradation

The curdlan samples weighting 20 ± 2 mg were placed in the 1.5 mL Eppendorf tubes containing 300 μL of degradation solution (HCl, pH = 4.5) or PBS (control). The tubes were placed in the cell culture incubator for 14 days. At determined time intervals (5, 7, 9, 11, and 14 days), the 20 μL of degradation solution or PBS were collected to estimate the concentration of glucose (degradation product) by colorimetric GOD-POD method using commercially available kit (Cormay, Poland). Additionally total carbohydrates in the solutions were detected by colorimetric Total Carbohydrate Assay Kit (Sigma-Aldrich Chemicals, Poland). After 14 days of incubation, the curdlan samples were air-dried and their weight loss was assessed using analytical balance. The degradation test was performed for three independent samples. An unpaired *t*-test was performed to evaluate statistically significant differences ($p < 0.05$) between HCl-treated curdlan matrices and control PBS-treated samples (GraphPad Prism 8.0.0 Software, USA).

2.5. ROS-mediated degradation of curdlan matrix

2.5.1. ROS/RNS generation by osteoclasts and immune cells

Neutrophils were isolated from human peripheral blood (informed consent was obtained from the volunteers) according to the previously described method (Wessely-Szponder et al., 2020; Zdziennicka et al., 2021). Red blood cell lysis was performed with 0.83 % ammonium chloride (Sigma-Aldrich Chemicals, Poland) followed by centrifugation at 700*g* for 15 min at 4 °C. The number and viability of neutrophils were evaluated using an R1 Automated Cell Counter (Olympus, Warsaw, Poland). The purity of isolated cells (estimated to be 85 % neutrophils) was confirmed by May-Grunewald-Giemsa staining (Sigma-Aldrich Chemicals, Poland). Then, the cells were suspended in PBS (Sigma-Aldrich Chemicals, Poland) and seeded at a density of 1×10^6 onto the curdlan gel placed in agarose-coated 24-multiwell plates. Monocytes and monocyte-derived macrophages were isolated from PBMCs collected from peripheral blood by gradient density centrifugation method as described in Section 2.2. The cells were seeded at a density of 1×10^6 onto the curdlan gel. Differentiation of monocytes towards mature macrophages was induced by addition of 25 ng/mL M-CSF (Sigma-Aldrich Chemicals, Poland) followed by 5-day culture at 37 °C with 5 % CO_2. Differentiation of monocytes towards mature osteoclasts was induced with M-CSF and RANKL as described in Section 2.2. Osteoclasts and immune cells (neutrophils, monocytes, and macrophages) seeded into the wells of 24-multiwell plate without curdlan matrix served as controls.

ROS/RNS generation was assessed after 24-h culture of neutrophils and monocytes on the curdlan gel, after 5-day culture in the case of macrophages, and after 7-day culture of osteoclasts. Assessment of superoxide (O_2^-) and nitrite (NO_2^-) generation was conducted according to the procedure reported in (Wessely-Szponder et al., 2020; Zdziennicka et al., 2021). Briefly, nitric oxide (NO) production was measured using the Griess reaction and calculated with a standard curve of different concentration of NO_2^- that is a stable product of NO in the medium. Superoxide production was evaluated by colorimetric method. The cells were incubated for 15 min with 0.1 % nitroblue tetrazolium solution (NBT, Sigma-Aldrich Chemicals, Poland) at room temperature and the absorbance was read at 545 nm. The generation of superoxide was calculated using the extinction coefficient of NBT (21.1 nM). An unpaired *t*-test was performed to evaluate statistically significant differences ($p < 0.05$) between control cells and immune cells seeded onto curdlan gel (GraphPad Prism 8.0.0 Software, USA).

2.5.2. Hydrogen peroxide effect on curdlan degradation

The effect of hydrogen peroxide (H_2O_2) on curdlan degradation was determined qualitatively by SEM imaging and quantitatively by evaluation of sugar release from the sample. The curdlan samples weighting 20 ± 2 mg were placed in the 1.5 mL Eppendorf tubes containing 300 μL of degradation solutions: (1) 1 μM H_2O_2 in PBS; (2) 1 mM H_2O_2 in PBS; (3) PBS (control). The tubes were placed in the cell culture incubator (37 °C, 5 % CO_2, 95 % humidity) for 7 days. At determined time intervals (2, 4, and 7 days), the 10 μL of degradation solution were collected to estimate the concentration of total carbohydrates (degradation product) by colorimetric Total Carbohydrate Assay Kit (Sigma-Aldrich Chemicals, Poland). After 7 days of incubation, the curdlan samples were air-dried and subjected to SEM imaging to observe microstructural changes. The degradation test was performed for three independent samples. One-way ANOVA followed by Tukey's test was used to calculate statistically significant differences ($p < 0.05$) between H_2O_2-treated curdlan matrices and control PBS-treated samples (GraphPad Prism 8.0.0 Software, USA).

3. Results and discussion

3.1.1. Osteoclast activity on curdlan gel

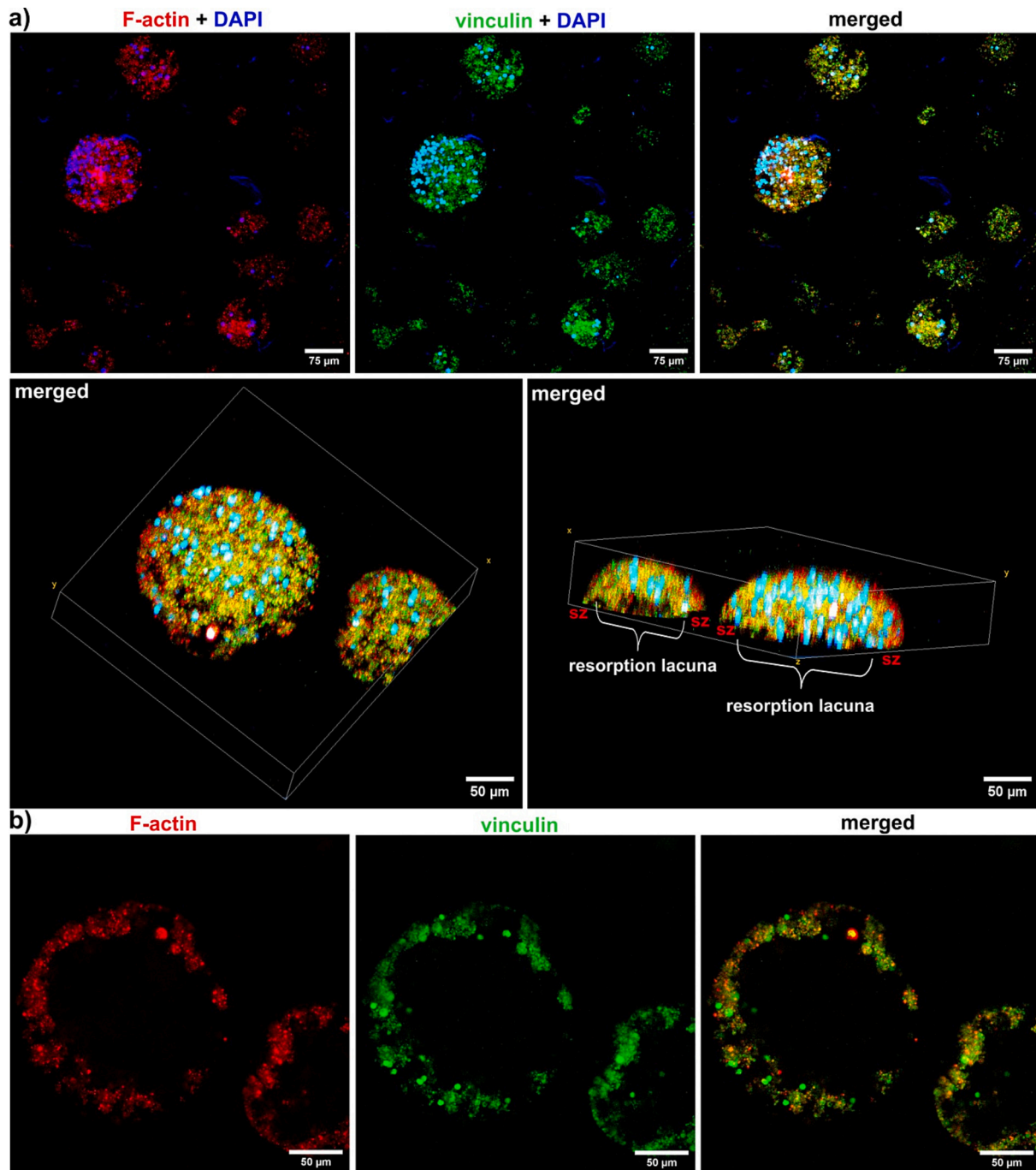Biomaterials for bone regeneration are expected to be bioabsorbed

Fig. 1. CLSM images and 3D models presenting active osteoclasts grown on the surface of the curdlan gel: a – osteoclast multinucleation (*sz* – sealing zone); b – actin belt.

after their implantation into the living organism. The main mechanism responsible for gradual replacement of bone implant by newly formed tissue is the resorption process that is mediated by osteoclasts. As osteoclasts significantly lower the pH in the resorption lacuna, it may be hypothesized that curdlan may be degraded after implantation by acidic hydrolysis. According to the available literature osteoclast differentiation and bone-resorbing function highly depends on the substrate stiffness. Thus, it is not surprising that substrates having higher stiffness (similar to the bone) promote osteoclast activity (Wang et al., 2022). Since curdlan gel is characterized by high elasticity and low stiffness, the primary aim of the study was to determine whether osteoclasts have the ability to attach to the curdlan matrix and differentiate towards mature bone-resorbing cells. CLSM observation revealed the presence of multinucleated giant cells with the typical morphology of osteoclasts (Fig. 1a). Multinucleation is a strong evidence of osteoclast maturation (Kodama & Kaito, 2020). Moreover, both fluorescent staining of actin belt (Fig. 1b) and TRAP immunohistochemistry (Fig. 2) confirmed the presence of mature TRAP-positive osteoclasts on the surface of curdlan gel. It should be noted that TRAP, which is an enzyme having the ability to degrade skeletal phosphoproteins (e.g. osteopontin), is considered to be a histochemical marker of mature bone-resorbing cells (Hayman, 2008). Importantly, active osteoclasts form a resorption complex that is made of an actin belt (or ring) that surrounds a so-called ruffled border containing vacuolar $H + $-ATPase, which is responsible for lowering the pH in the resorption lacuna. The actin belt is actually the area of tight connection between the osteoclast plasma membrane and the bone surface (Han et al., 2019). It was also proven that some focal adhesion proteins, like vinculin and talin, participate in the formation of actin belt. Lakkakorpi et al. demonstrated that actin belt in the active osteoclasts is in fact formed by F-actin ring located between the double circle of vinculin found in the periphery of the cell. They also proved that F-actin/vinculin/talin zones correspond to the resorption lacuna edge and are necessary for osteoclast attachment and bone-resorbing activity (Lakkakorpi et al., 1989). Obtained CLSM images clearly showed the presence of both F-actin and vinculin circles within the actin belt, proving resorption activity of the osteoclasts grown on the curdlan gel (Fig. 1b).

3.2. Determination of osteoclast-mediated curdlan hydrolysis

To prove the ability of osteoclasts to degrade thermally gelled curdlan, the samples upon osteoclast culture were subjected to osmotic lysis to remove the cells followed by microscopy and spectroscopy analyses. Microscopy observation with the use of AFM and SEM of curdlan surface

after osteoclast culture clearly showed the intact areas characterized by smooth surface (similar to the surface of unseeded control sample incubated in the culture medium) and rough topography that was created by the osteoclast activity (Figs. 3 and 4a). Importantly, AFM observation revealed that the activity of osteoclasts resulted in an important roughening (Fig. 3b) of the surface, in contrast with the flat and smooth of the control polymer surface (Fig. 3a). In fact, the average roughness Ra increased from 1.47 nm in the control sample, to 20.50 nm in the cell-treated curdlan due to the osteoclastic activity (measurements parameters can be seen in Supplementary Material 2).

To confirm acidic hydrolysis of curdlan matrix, the degradation test in the conditions mimicking that occurring in the resorption lacuna during osteoclast-mediated degradation was performed using cell-free system. After bone scaffold implantation, osteoclasts adhere to the biomaterial surface and form a resorption lacuna. The pH within the lacuna is lowered to about 4.0–4.5 by the release of protons (proton pump and Na^+–H^+ exchanger) and chloride ions (chloride channels) (Henriksen et al., 2008; Low & Kopeček, 2012). Therefore, to simulate acidic environment that is locally formed by osteoclasts, HCl degradation solution with pH equal to 4.5 was prepared. Unseeded curdlan samples were placed in the degradation solution and PBS (control) followed by incubation in the conditions mimicking physiological ones: 37 °C, 5 % CO_2, 95 % humidity, without agitation. SEM imaging performed after 14-day incubation showed similar results like for osteoclast-seeded curdlan samples. HCl-treated sample was characterized by rough surface, whereas control PBS-treated matrix exhibited smooth and intact surface (Fig. 4b). Importantly, surface of both culture medium- and PBS-treated control was smooth and similar to the surface of untreated control sample (native curdlan gel, Fig. 4c), proving that observed changes were related to acidic hydrolysis caused by either osteoclasts (Fig. 4a) or HCl (Fig. 4b). Slight changes in topography of control samples compared to native curdlan gel resulted from either adsorption of the proteins (culture medium-treated sample) or salt precipitation (PBS-treated sample).

Moreover, to quantitatively determine curdlan hydrolysis in the environment mimicking resorption lacuna, the concentration of glucose (degradation product) was assessed. The test clearly showed the increase in glucose concentration in the degradation solution (HCl) with time (Table 1). Curdlan gel incubated in PBS also released some glucose but its level was constant through the full length of the experiment. In the case of total carbohydrate assay, curdlan sample treated with HCl released great amounts of sugars, whereas concentration of carbohydrates in PBS was slightly higher than the concentration of glucose and it was constant through the full length of the experiment. Thus, it was
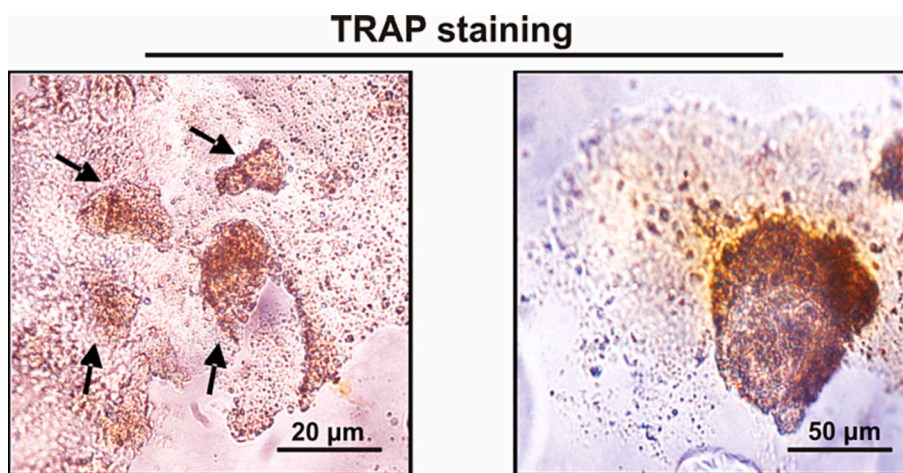

Fig. 2. Microscope images presenting mature TRAP-positive osteoclasts (brownish color) grown on the surface of curdlan gel (on the left – lower magnification image showing curdlan gel covered by a number of active osteoclasts indicated by black arrows; on the right – higher magnification image presenting single TRAP-positive osteoclast).
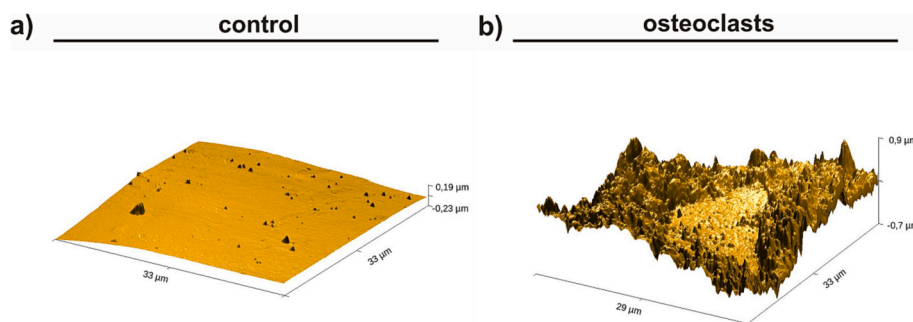
Fig. 3. AFM images presenting surface of the curdlan samples: a – control of unseeded curdlan incubated in culture medium; b – curdlan after 14-day osteoclast culture.

assumed that the presence of sugars in the PBS was not a result of curdlan degradation, but it was a contamination of the curdlan powder used for the matrix production. It is worth noting that glucose and sucrose are the main carbon sources used for microbial synthesis of curdlan (Aquinas et al., 2021). Greater amounts of total carbohydrates compared to glucose in HCl degradation solution indicated either contamination of the curdlan powder with sucrose or the presence of oligosaccharides due to acidic hydrolysis of the sample. Substantial degradation of the curdlan during 14-day incubation in HCl solution was proven by significant weight loss (by 58 ± 6 %) of the sample. Control PBS-treated sample exhibited weight loss by only 11 ± 4 %.

Chemical changes on the surface of curdlan gel after osteoclast culture and incubation in HCl degradation solution were analysed by Raman spectroscopy. Initially, series of single spectra were collected from rough and smooth areas after osteoclast culture as presented in Fig. 4, alongside from HCl-treated and control samples. Recorded spectra were averaged and normalized to 2905 cm^{-1} band and presented in Fig. 5a. Overlayed average Raman spectra of osteoclast- and HCl-treated curdlan matrix may be seen in Supplementary Material 3. Most distinguish shifts were identified in the range of 800–1500 cm^{-1}, consisting of vibrations assigned to CC and CO stretching, vibrations of C—O—C glycosidic bond, in plane ring deformation, OH and CH bending and eventually CH$_2$ in-plane bending in CH$_2$OH group (Gieroba et al., 2020). As mentioned above, hydrolysis of curdlan resulted in higher concentration of glucose after breaking glycosidic bonds between monomers (Prieto et al., 2011). Bands assigned to β-glycosidic bonds are recognizable at 888 cm^{-1} (HCC, HCO, CH deformational out-of-plane), 1093 with a shoulder band at 1148 cm^{-1} (C—O—C stretching) and in range 1200–1300 cm^{-1}. In Fig. 5b Raman shifts in samples exposed to osteoclasts and HCl can be seen around 1460 and 1045 cm^{-1} were assigned to CH$_2$ in-plane bending, CC, COH, CH deformation respectively. This suggests that during acidic hydrolysis the bands were broken at random places in the polysaccharide chain, releasing maltodextrin molecules, apart from glucose (de Veij et al., 2009). In both biological (osteoclast-mediated) and chemical (cell-free) degradation tests, second derivative revealed presence of the band at 1433 and 1448 cm^{-1} that can be assigned to rocking of CH and deformation of CH$_2$ of carbohydrate monomers (Wiercigroch et al., 2017). It was also noticed by shifts around 1460 cm^{-1} and appearing new bands at 1072 cm^{-1} (osteoclasts) or at 1085 and 1089 cm^{-1} (HCl) derived from appearing monosaccharides and disaccharides.

To properly describe the curdlan degradation process, bands at 888 and 2905 cm^{-1} were chosen, assigned to β-glycosidic bond and CH$_2$ stretching of aliphatic chain vibration, respectively. Raman intensity ratio of these bands ($R_h = I_{888}:I_{2905}$) was calculated from spectra and subjected to unpaired *t*-test, when statistical significance ($p < 0.05$) for difference was confirmed. It was later implemented in analysis of Raman maps, as a spatial visualization, presented in Fig. 6. To exclude the influence of various manipulations during experiment, additional control groups were analysed with Raman imaging. The culture medium-treated

and PBS-treated curdlan samples were controls for osteoclast-mediated degradation test (Fig. 6a) and cell-free system experiment performed in HCl (Fig. 6b), respectively. Raman image of untreated curdlan gel – native sample (Fig. 6c) was considered as negative control revealing no chemical changes. For visualization of microscopic image, β-glycosidic bonds, CH$_2$ of aliphatic chains content, R_h and carbohydrates were chosen for HCl- and cell-treated curdlan samples. Carbohydrates were presented with region I (200–800 cm^{-1}) (Wiercigroch et al., 2017), as expected that hexoses and disaccharides composed of hexose were present from the previous experiments data. In Fig. 6a, heatmap of $R_h = I_{888}:I_{2905}$ revealed distinguishable area of lower ratio values, marked in blue, assigned to rough surface areas (marked with letter 'r'). The shape appearing at the bottom of chemical map resulting from degradation of curdlan matrix resembled the shape and size of osteoclasts shown in Figs. 1 and 2. For better visualization of process semi-quantitative evaluation of glucose concentration in resorption lacuna was performed. Similarly, to R_h the higher concentration of carbohydrates resembled the lacuna edge, and varied in sample treated with cells, comparing to HCl-treated one (Fig. 6b). In both control samples (culture medium- and PBS-treated) no effects resembling those induced by osteoclasts were observed. However, higher Raman intensity in carbohydrates in PBS sample was observed due to overlapping bands of phosphate buffer in ranges near ~206 cm^{-1} and 462 cm^{-1}, which is known phenomenon (Baranov et al., 2010).

The Raman map of HCl-treated curdlan matrix showed quite evenly distributed carbohydrates and lack of outlining areas, as the whole mapped sample was staying in contact with HCl, which also corresponds with SEM images (Fig. 6b). Interestingly, comparison with the Raman intensity of carbohydrates in maps obtained for osteoclast-treated samples (Fig. 6a) and HCl-treated matrix (Fig. 6b) may suggest that chemical hydrolysis of curdlan in the cell-free system was less efficient than osteoclast-mediated process, but further, more quantitative analyses are needed to confirm this assumption. Similarly to carbohydrates, but in contrary to data shown in Fig. 6a, the distribution of R_h is even, not showing any recognizable cell-shaped structures. It should be noted that osteoclasts, similarly to immune cells, may generate ROS/RNS that facilitate resorption of bone tissue during remodeling (Agidigbi & Kim, 2019). Thus, it may be assumed that more efficient curdlan hydrolysis upon osteoclast culture compared to HCl-treated sample could have resulted from enhanced degradation process due to ROS/RNS generation by the cells.

3.3. Determination of ROS-mediated curdlan degradation

It is known that implanted biomaterials may exert inflammatory response and activate immune cells to generate excessive amounts of ROS/RNS. Consequently, prolonged inflammation may result in oxidative damage of the implant and its failure (Przekora, 2019). Within this study, curdlan-induced ROS/RNS generation by immune cells (neutrophils, monocytes, and macrophages) was determined. Neutrophils and
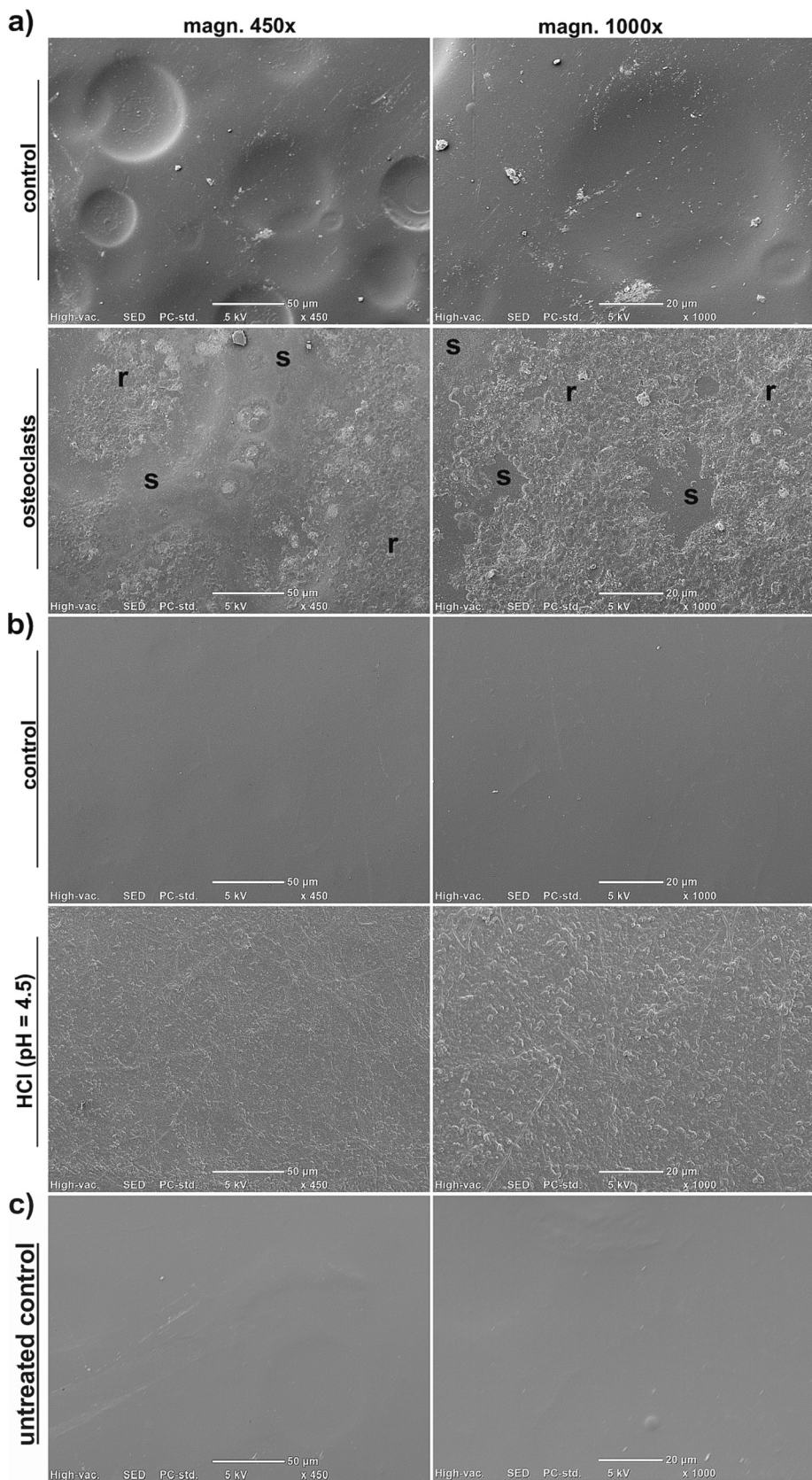
Fig. 4. SEM images presenting surface of the curdlan samples: a – osteoclast-mediated degradation of curdlan sample (control – unseeded curdlan gel incubated in culture medium; osteoclasts – sample after 14-day culture of bone-resorbing cells: s – smooth intact area; r – rough degraded area); b – cell-free chemical degradation test in the environment mimicking resorption lacuna (control – unseeded sample incubated in PBS; HCl (pH = 4.5) – unseeded sample incubated in HCl degradation solution); c – untreated curdlan gel (native sample).

Table 1

Degradation of curdlan matrix in the environment mimicking resorption lacuna determined by measurement of glucose and total carbohydrates concentration in the degradation solution (HCl) and PBS (control).

Concentration of released glucose [µg/mL]				
	5 days	7 days	9 days	11 days	14 days
PBS	30.38 ± 7.71	34.32 ± 0.28	37.30 ± 4.04	38.09 ± 8.25	37.56 ± 8.13
HCl	59.95 ± 4.15[a]	82.64 ± 12.58[a]	80.64 ± 13.29[a]	86.85 ± 4.07[a]	94.41 ± 3.50[a]

Concentration of released total carbohydrates [µg/mL]				
	5 days	7 days	9 days	11 days	14 days
PBS	41.39 ± 0.23	42.67 ± 2.14	45.86 ± 1.13	45.65 ± 1.18	42.25 ± 2.17
HCl	71.74 ± 2.51[a]	91.25 ± 2.40[a]	102.90 ± 3.99[a]	110.80 ± 0.90[a]	117 ± 2.77[a]

[a] Statistically significant results compared to the control sample incubated in PBS ($p < 0.05$, unpaired *t*-test).

monocytes cultured on the curdlan sample produced significantly higher amounts of ROS and RNS (on the basis of superoxide and NO generation, respectively) in comparison with corresponding control cells cultured without curdlan matrix (Fig. 7a). It is not surprising since β-glucans (including curdlan) are known to have immunomodulatory properties with the ability to enhance activity of immune cells (Ali et al., 2015; Kataoka et al., 2002; Ratitong et al., 2021). For instance, De Souza Bonfim-Mendonca et al. demonstrated that β-glucan derived from *Laminaria digitata* induced ROS production in human neutrophils (De Souza Bonfim-Mendonça et al., 2014). Ulvestad et al. observed increased production of superoxide and NO by macrophages stimulated with curdlan (Ulvestad et al., 2018). Similarly, Żelechowska et al. found out that curdlan not only acted as a chemoattractant for mast cells, but also stimulated those cells to produce elevated ROS (Żelechowska et al., 2020). Whereas Kataoka et al. detected increased expression of inducible nitric oxide synthase (iNOS – an enzyme producing NO) in curdlan-treated mouse macrophages (Kataoka et al., 2002). Nevertheless, in our studies thermally gelled curdlan was used – known to have reduced immunomodulatory properties compared to curdlan solution (Kataoka et al., 2002) – therefore production of ROS/RNS by neutrophils and monocytes was only slightly promoted, however with statistical significance. Macrophages cultured on the curdlan gel showed comparable NO production and slightly lower generation of superoxide compared to control macrophages incubated without curdlan sample.

Since it is known that osteoclasts release ROS/RNS enhancing bone resorption (Agidigbi & Kim, 2019), production of superoxide and NO by osteoclasts cultured on the curdlan gel was also determined. Osteoclasts grown on the tested sample gave similar results to macrophages, i.e.
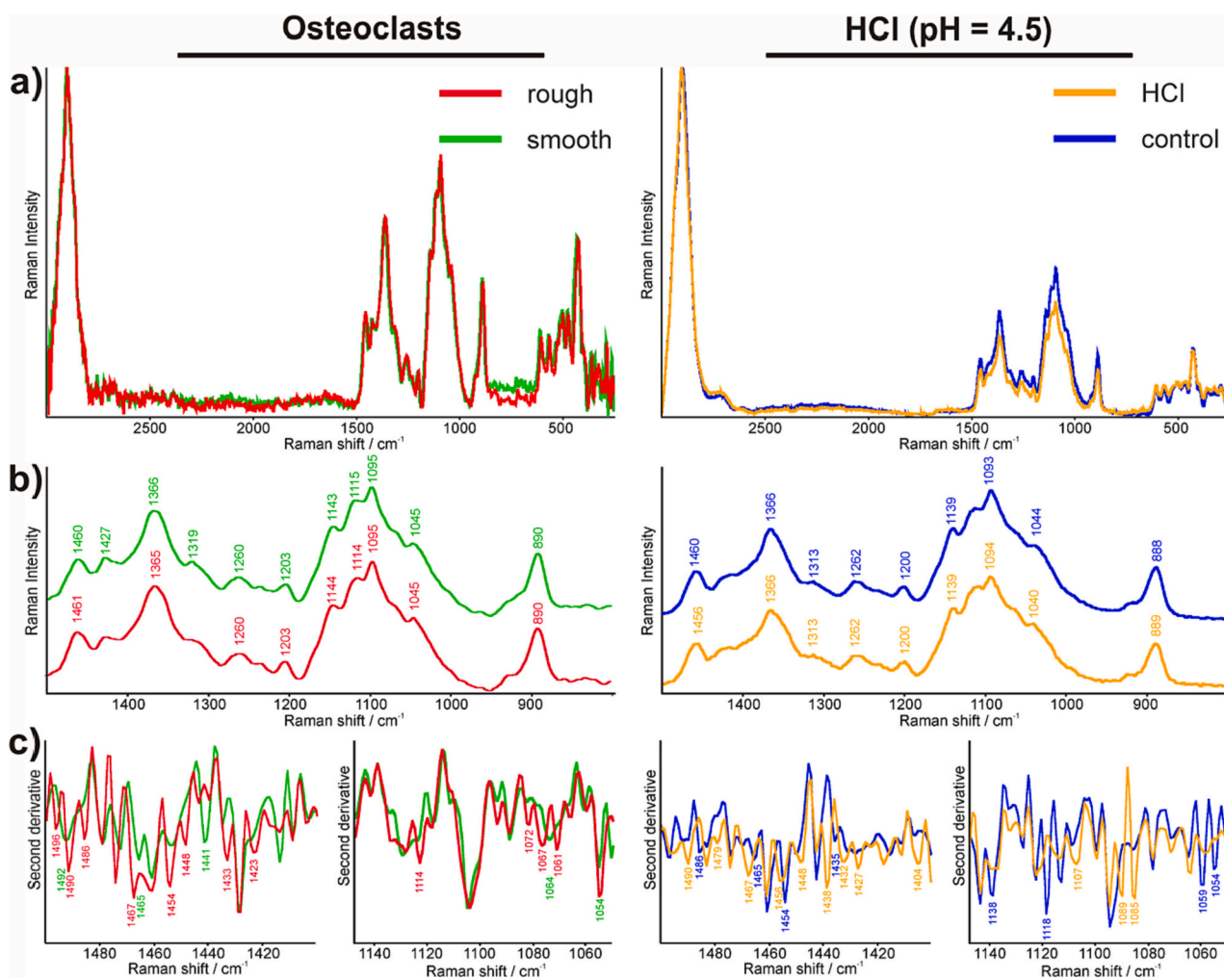

Fig. 5. Raman spectra of curdlan matrix after osteoclast-mediated degradation (on the left) and cell-free chemical degradation in the environment mimicking resorption lacuna (on the right): a – spectra in range 200–3000 cm⁻¹ normalized to 2905 cm⁻¹ band, b – range 800–1500 cm⁻¹ with ascribed maxima of bands, c – second derivative spectra of ranges 1400–1500 cm⁻¹ and 1040–1140 cm⁻¹ with ascribed most distinguish differences between samples.
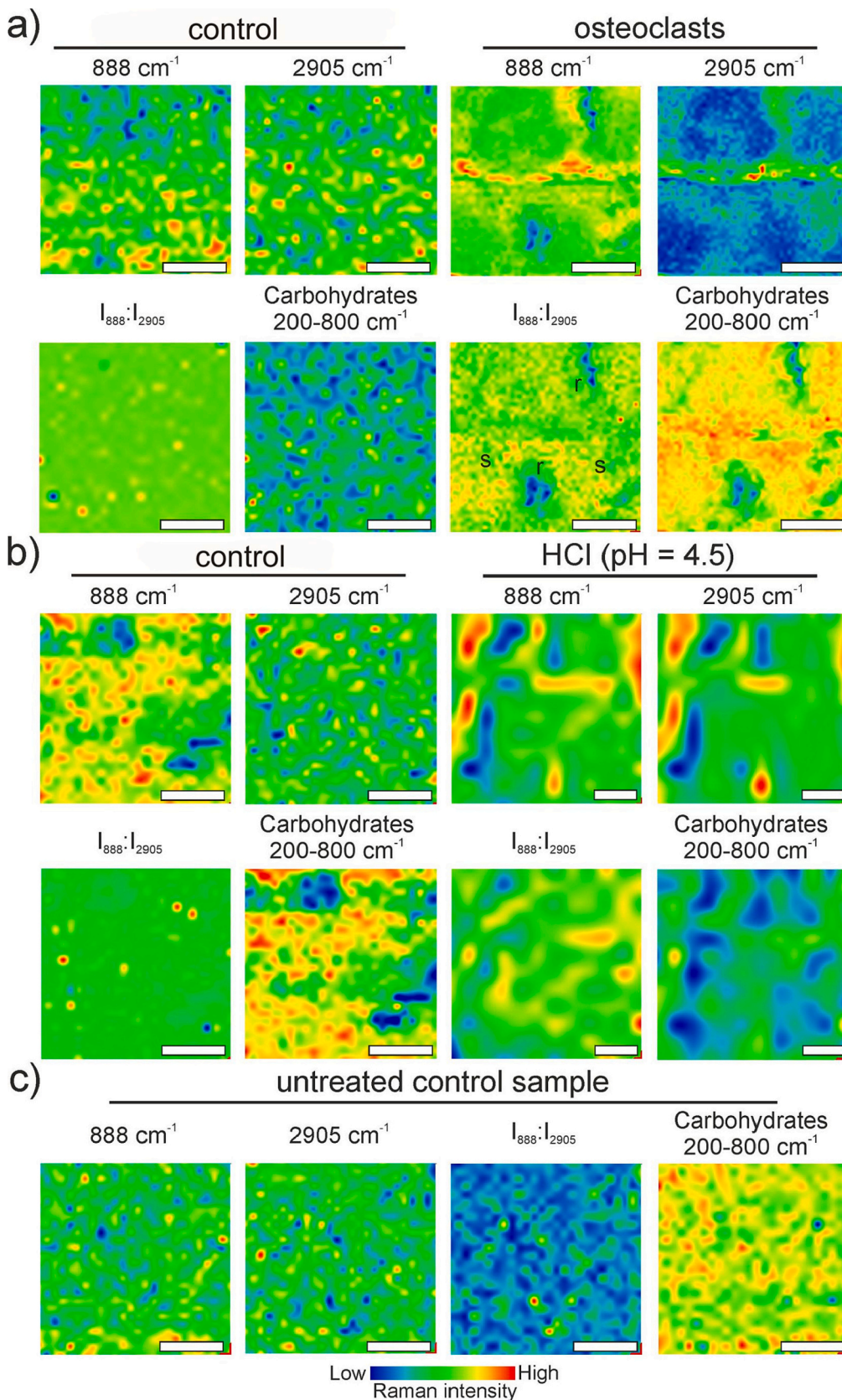
Fig. 6. Chemical Raman images of curdlan samples: a – osteoclast-mediated degradation (control – unseeded curdlan gel incubated in culture medium; osteoclasts – sample after 14-day culture of bone-resorbing cells: s – smooth intact area; r – rough degraded area; white bars represent 50 μm), b – cell-free chemical degradation test in the environment mimicking resorption lacuna (control – unseeded sample incubated in PBS; HCl (pH = 4.5) – unseeded sample incubated in HCl degradation solution; white bars represent 5 μm), c – untreated (native) curdlan gel (white bars represent 50 μm).
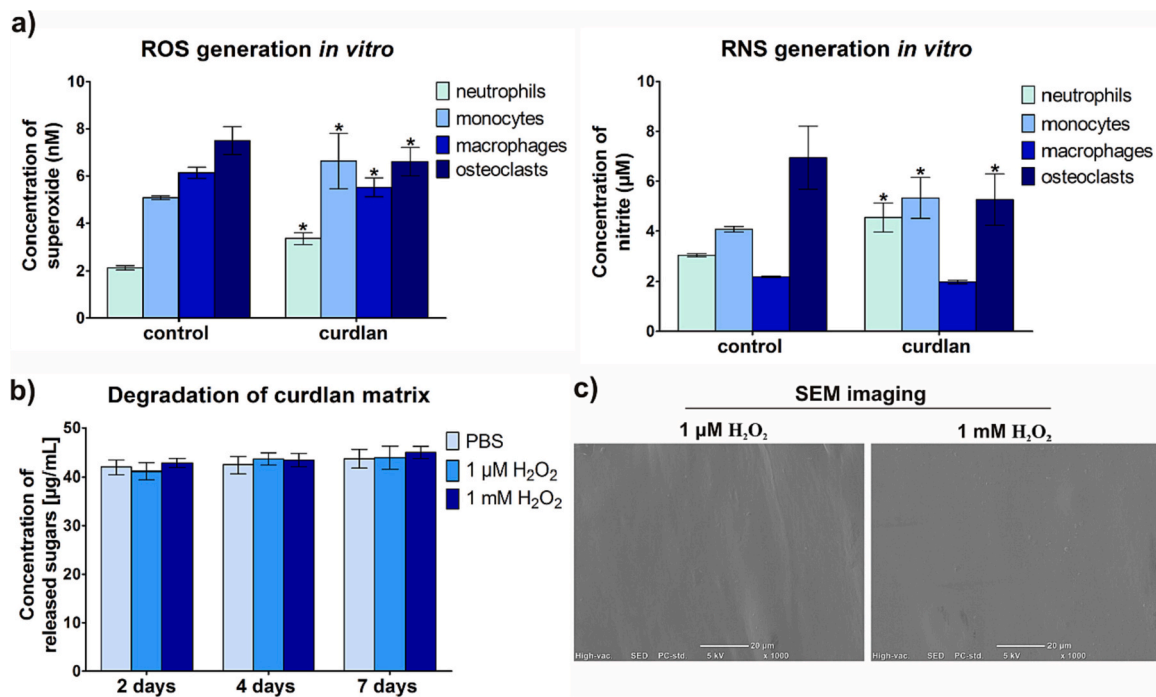
Fig. 7. ROS-mediated degradation of curdlan gel: a – ROS/RNS generation by immune cells and osteoclasts (control – cells cultured without curdlan sample; curdlan – cells cultured on the tested sample; * statistically significant results compared to corresponding control cells, $p < 0.05$, unpaired *t*-test); b – degradation of curdlan matrix in H_2O_2 solutions determined by measurement of released total carbohydrates (PBS – control solution without H_2O_2); c – SEM images presenting surface of the curdlan after incubation in H_2O_2 solutions (white bars represent 20 μm; surface of the control sample after incubation in PBS and untreated curdlan sample may be seen in Fig. 4b and c, respectively).

they produced slightly lower amounts of ROS/RNS compared to the control cells (Fig. 7a). Thus, thermally gelled curdlan did not have the ability to enhance ROS/RNS generation by active osteoclasts.

Although differences in ROS/RNS production between cells cultured on the curdlan gel and control cells were slight, even physiological level of reactive oxygen species may contribute to curdlan degradation. To check the ability of ROS to degrade thermally gelled curdlan, the sample was exposed to hydrogen peroxide (H_2O_2). It should be noted that H_2O_2 was proven to be involved in the ROS-mediated degradation of beta-glucans (Faure, Werder, & Nyström, 2013). The experiment demonstrated that H_2O_2 did not participate in the degradation of thermally gelled curdlan as tested sample did not release augmented levels of carbohydrates (measured by Total Carbohydrate Assay kit) after incubation in H_2O_2 solutions compared to the control incubated in PBS (Fig. 7b). Moreover, there were no differences in the amount of released carbohydrates between low (1 μM) and high (1 mM) concentration of H_2O_2 in the degradation solution. SEM imaging confirmed that exposure of curdlan to H_2O_2 solutions did not lead to its degradation as no changes in curdlan microstructure were observed (Fig. 7c). Thus, the experiment clearly showed that H_2O_2 itself did not have the ability to degrade curdlan gel. Therefore, immune cells most likely would not be able to damage thermally gelled curdlan by ROS/RNS release upon biomaterial implantation. However, combination of acidified microenvironment in the resorption lacuna with ROS generated by osteoclasts may potentially enhance chemical hydrolysis, which had the reflection in Raman imaging that showed greater hydrolysis of curdlan after osteoclasts culture compared to HCl-treated sample (Fig. 6a and b).

4. Conclusions

Curdlan is the component of many recently developed bone implants, including commercial ones (FlexiOss®, Medical Inventi, Poland). Since human organism does not produce enzymes having the ability to degrade curdlan, it is not clear what is the fate of thermally gelled curdlan after its implantation into the bone. Within this research it was clearly shown that osteoclasts may easily adhere to the surface of the curdlan gel and acidify microenvironment leading to its degradation by acidic hydrolysis. Osteoclast culture on the surface of curdlan gel resulted in noticeably changed topography manifested by increased roughness as demonstrated by SEM and AFM imaging. Moreover, curdlan degradation was proven by detection of chemical changes by Raman spectroscopy. Both Raman spectra and chemical Raman images obtained for osteoclast-treated samples clearly indicated acidic hydrolysis of the curdlan. Moreover based on obtained results it may be assumed that combination of ROS/RNS produced by osteoclasts with acidified microenvironment in the resorption lacuna will most likely boost curdlan degradation. Therefore presented studies for the first time provide a strong evidence of osteoclast-mediated acidic hydrolysis of thermally obtained curdlan gel, which is a very important issue taking into account clinical applications of curdlan-based biomaterials. However, it should be noted that many other cell types (including immune cells such as macrophages, neutrophils, dendritic cells) are involved in bone remodeling after biomaterial implantation. Thus, other factors like oxidative stress caused by excessive ROS/RNS generation by immune cells in response to biomaterial may also have impact on curdlan degradation. Within this study it was proven that immune cells (but not osteoclasts) produced slightly increased amounts of ROS/RNS in contact with curdlan gel. However, even ROS/RNS production at physiological level may potentially enhance curdlan degradation mediated by osteoclasts. To reliably determine the effect of ROS/RNS release by immune cells on osteoclast-mediated degradation of curdlan, more complex cellular model is needed such as co-culture system. Nevertheless, both macrophages and osteoclasts are derived from monocytes, thus it is huge challenge to establish co-culture system *in vitro* to test osteoclast-mediated degradation of curdlan in more complex microenvironment.

Supplementary data to this article can be found online at https://doi.org/10.1016/j.carbpol.2022.119914.

CRediT authorship contribution statement

The manuscript was written through contributions of all authors. All authors have given approval to the final version of the manuscript.

AP: Conceptualization, Methodology, Investigation, Data analysis, Resources, Project administration, Supervision, Writing – original draft; LP: Investigation, Methodology, Data visualization, Data analysis, Writing – review & editing; GK: Investigation, Methodology, Data visualization, Data analysis, Writing – original draft; PK: Investigation, Methodology, Data visualization, Data analysis, Writing – review & editing; CC: Investigation, Data visualization, Writing – review & editing; MW: Investigation, Data visualization; RP: Resources, Supervision, Writing – review & editing; ASB: Resources, Supervision, Writing – review & editing.

Data availability

The raw/processed data required to reproduce these findings can be obtained from the corresponding author (agata.przekora@umlub.pl) upon reasonable request.

Declaration of competing interest

The authors declare that they have no known competing financial interests or personal relationships that could have appeared to influence the work reported in this paper.

Data availability

Data will be made available on request.

References

Agidigbi, T. S., & Kim, C. (2019). Reactive oxygen species in osteoclast differentiation and possible pharmaceutical targets of ROS-mediated osteoclast diseases. *International Journal of Molecular Sciences, 20*(14), 3576. https://doi.org/10.3390/ijms20143576

Ali, M. F., Driscoll, C. B., Walters, P. R., Limper, A. H., & Carmona, E. M. (2015). Beta-glucan-activated human B lymphocytes participate in innate immune responses by releasing proinflammatory cytokines and stimulating neutrophil chemotaxis. *The Journal of Immunology, 195*(11), 5318–5326. https://doi.org/10.4049/jimmunol.1500559

Aquinas, N., Selvaraj, S., & Bhat, M. R. (2021). A review presenting production, characterization, and applications of biopolymer curdlan in food and pharmaceutical sectors. *Polymer Bulletin*. https://doi.org/10.1007/s00289-021-03860-1

Baranov, A. V., Bogdanov, K. V., Ushakova, E. V., Cherevkov, S. A., Fedorov, A. V., & Tscharntke, S. (2010). Comparative analysis of Raman spectra of PbS macro- and nanocrystals. *Optics and Spectroscopy, 109*(2), 268–271. https://doi.org/10.1134/s0030400x10080199

Borkowski, L., Przekora, A., Belcarz, A., Palka, K., Jojczuk, M., Lukasiewicz, P. Ginalska, G., … (2021). Highly porous fluorapatite/β-1,3-glucan composite for bone tissue regeneration: Characterization and in vitro assessment of biomedical potential. *International Journal of Molecular Sciences, 22*(19), 10414. https://doi.org/10.3390/ijms221910414

Chaudhari, V., Buttar, H. S., Bagwe-Parab, S., Tuli, H. S., Vora, A., & Kaur, G. (2021). Therapeutic and industrial applications of curdlan with overview on its recent patents. *Frontiers in Nutrition, 28*(8), Article 646988. https://doi.org/10.3389/fnut.2021.646988

De Souza Bonfim-Mendonça, P., Ratti, B. A., Da Silva Ribeiro Godoy, J., Negri, M., De Lima, N. C. A., Fiorini, A., & Svidzinski, T. I. E. (2014). β-Glucan induces reactive oxygen species production in human neutrophils to improve the killing of Candida albicans and Candida glabrata isolates from vulvovaginal candidiasis. *PLoS ONE, 9* (9), Article 9. https://doi.org/10.1371/journal.pone.0107805

Diez-Escudero, A., Espanol, M., Montufar, E. B., Di Pompo, G., Ciapetti, G., Baldini, N., & Ginebra, M. P. (2017). Focus ion beam/scanning electron microscopy characterization of osteoclastic resorption of calcium phosphate substrates. *Tissue Engineering - Part C: Methods, 23*(2), 118–124. https://doi.org/10.1089/ten.tec.2016.0361

Diez-Escudero, A., Torreggiani, E., Di Pompo, G., Espanol, M., Persson, C., Ciapetti, G. Ginebra, M. P., … (2019). Effect of calcium phosphate heparinization on the in vitro inflammatory response and osteoclastogenesis of human blood precursor cells. *Journal of Tissue Engineering and Regenerative Medicine, 13*(7), 1217–1229. https://doi.org/10.1002/term.2872

Everts, V., Korper, W., Hoeben, K. A., Jansen, I. D. C., Bromme, D., Cleutjens, K. B. J. M. Beertsen, W., … (2006). Osteoclastic bone degradation and the role of different cysteine proteinases and matrix metalloproteinases: Differences between calvaria and long bone. *Journal of Bone and Mineral Research, 21*(9), 1399–1408. https://doi.org/10.1359/jbmr.060614

Faure, A. M., Werder, J., & Nyström, L. (2013). Reactive oxygen species responsible for beta-glucan degradation. *Food Chemistry, 141*, 589–596. https://doi.org/10.1016/j.foodchem.2013.02.096

Gidley, M., & Nishinari, K. (2009). Physico-chemistry of (1,3)-β-glucans. In A. Bacic, G. Fincher, & B. Stone (Eds.), *Chemistry, biochemistry and biology of (1,3)-β-glucans and related polysaccharides* (pp. 47–118). New York: Academic Press (Elsevier). https://doi.org/10.1016/B978-0-12-373971-1.00003-0.

Gieroba, B., Sroka-Bartnicka, A., Kazimierczak, P., Kalisz, G., Pieta, I. S., Nowakowski, R., & Przekora, A. (2020). Effect of gelation temperature on the molecular structure and physicochemical properties of the curdlan matrix: Spectroscopic and microscopic analyses. *International Journal of Molecular Sciences, 21*(17), 6154. https://doi.org/10.3390/ijms21176154

Han, G., Zuo, J., & Holliday, L. S. (2019). Specialized roles for actin in osteoclasts: Unanswered questions and therapeutic opportunities. *Biomolecules, 9*(17). https://doi.org/10.3390/biom9010017

Hayman, A. (2008). Tartrate-resistant acid phosphatase (TRAP) and the osteoclast/immune cell dichotomy. *Autoimmunity, 41*(3), 218–223. https://doi.org/10.1080/08916930701694667

Henriksen, K., Sørensen, M. G., Jensen, V. K., Dziegiel, M. H., Nosjean, O., & Karsdal, M. A. (2008). Ion transporters involved in acidification of the resorption lacuna in osteoclasts. *Calcified Tissue International, 83*(3), 230–242. https://doi.org/10.1007/s00223-008-9168-8

Kataoka, K., Muta, T., Yamazaki, S., & Takeshige, K. (2002). Activation of macrophages by linear (1→3)-β-D-glucans. Implications for the recognition of fungi by innate immunity. *Journal of Biological Chemistry, 277*(39), 36825–36831. https://doi.org/10.1074/jbc.M206756200

Klimek, K., Przekora, A., Benko, A., Niemiec, W., Blazewicz, M., & Ginalska, G. (2017). The use of calcium ions instead of heat treatment for β-1,3-glucan gelation improves biocompatibility of the β-1,3-glucan/HA bone scaffold. *Carbohydrate Polymers, 164*. https://doi.org/10.1016/j.carbpol.2017.02.015

Kodama, J., & Kaito, T. (2020). Osteoclast multinucleation: Review of current literature. *International Journal of Molecular Sciences, 21*(16), 5685. https://doi.org/10.3390/ijms21165685

Lakkakorpi, P., Tuukkanen, J., Hentunen, T., Järvelin, K., & Väänänen, K. (1989). Organization of osteoclast microfilaments during the attachment to bone surface in vitro. *Journal of Bone and Mineral Research, 4*(6), 817–825. https://doi.org/10.1002/jbmr.5650040605

Laxmi, V. M., Latha, D., & Jayasree, A. S. (2018). Production and characterization of curdlan from Agrobacterium sp. *International Journal of Pharmaceutical Sciences and Research, 9*(11), 4871–4874. https://doi.org/10.13040/IJPSR.0975-8232.9 (11).4871-74

Leong, K. F., Chua, C. K., Sudarmadji, N., & Yeong, W. Y. (2008). Engineering functionally graded tissue engineering scaffolds. *Journal of the Mechanical Behavior of Biomedical Materials, 1*(2), 140–152. https://doi.org/10.1016/j.jmbbm.2007.11.002

Low, S. A., & Kopeček, J. (2012). Targeting polymer therapeutics to bone. *Advanced Drug Delivery Reviews, 64*(12), 1189–1204. https://doi.org/10.1016/j.addr.2012.01.012

Mangolim, C. S., Da Silva, T. T., Fenelon, V. C., Koga, L. N., De Ferreira, S. B. S., Bruschi, M. L., & Matioli, G. (2017). Description of recovery method used for curdlan produced by Agrobacterium sp. IFO 13140 and its relation to the morphology and physicochemical and technological properties of the polysaccharide. *PLoS ONE, 12* (2), Article e0171469. https://doi.org/10.1371/journal.pone.0171469

Martinez, C. O., Ruiz, S. P., Nogueira, M. T., Bona, E., Portilho, M., & Matioli, G. (2015). Effective immobilization of Agrobacterium sp. IFO 13140 cells in loofa sponge for curdlan biosynthesis. *Molecules, 20*(5), 7957–7973. https://doi.org/10.3390/molecules20057957

Matsuzaki, K., Katayama, K., Takahashi, Y., Nakamura, I., Udagawa, N., Tsurukai, T. Suda, T., … (1999). Human osteoclast-like cells are formed from peripheral blood mononuclear cells in a coculture with SaOS-2 cells transfected with the parathyroid hormone (PTH)/PTH-related receptor gene. *Endocrinology, 140*(2), 925–932. https://doi.org/10.1210/endo.140.2.6573

Michalicha, A., Roguska, A., Przekora, A., Budzyńska, B., & Belcarz, A. (2021). Poly (levodopa)-modified β-glucan as a candidate for wound dressings. *Carbohydrate Polymers, 272*, Article 118485. https://doi.org/10.1016/j.carbpol.2021.118485

Prieto, M. A., Vázquez, J. A., & Murado, M. A. (2011). Hydrolysis optimization of mannan, curdlan and cell walls from endomyces fibuliger grown in mussel processing wastewaters. *Process Biochemistry, 46*(8), 1579–1588. https://doi.org/10.1016/j.procbio.2011.04.014

Przekora, A. (2019). The summary of the most important cell-biomaterial interactions that need to be considered during in vitro biocompatibility testing of bone scaffolds for tissue engineering applications. *Materials Science and Engineering C, 97*. https://doi.org/10.1016/j.msec.2019.01.061

Przekora, A., & Ginalska, G. (2014). Addition of 1,3-β-d-glucan to chitosan-based composites enhances osteoblast adhesion, growth, and proliferation. *International Journal of Biological Macromolecules, 70*, 474–481. https://doi.org/10.1016/j.ijbiomac.2014.07.035

Przekora, A., & Ginalska, G. (2016). In vitro evaluation of the risk of inflammatory response after chitosan/HA and chitosan/β-1,3-glucan/HA bone scaffold implantation. *Materials Science and Engineering C, 61*, 355–361. https://doi.org/10.1016/j.msec.2015.12.066

Przekora, A., Vandrovcova, M., Travnickova, M., Pajorova, J., Molitor, M., Ginalska, G., & Bacakova, L. (2017). Evaluation of the potential of chitosan/β-1,3-glucan/hydroxyapatite material as a scaffold for living bone graft production in vitro by comparison of ADSC and BMDSC behaviour on its surface. *Biomedical Materials (Bristol), 12*(1). https://doi.org/10.1088/1748-605X/aa56f9

Ratitong, B., Marshall, M., & Pearlman, E. (2021). β-Glucan-stimulated neutrophil secretion of IL-1α is independent of GSDMD and mediated through extracellular vesicles. *Cell Reports, 35*(7), Article 109139. https://doi.org/10.1016/j.celrep.2021.109139

Sun, Y., Liu, Y., Li, Y., Lv, M., Li, P., Xu, H., & Wang, L. (2011). Preparation and characterization of novel curdlan/chitosan blending membranes for antibacterial applications. *Carbohydrate Polymers, 84*(3), 952–959. https://doi.org/10.1016/j.carbpol.2010.12.055

Tukulula, M., Hayeshi, R., Fonteh, P., Meyer, D., Ndamase, A., Madziva, M. T.Dube, A., … (2015). Curdlan-conjugated PLGA nanoparticles possess macrophage stimulant activity and drug delivery capabilities. *Pharmaceutical Research, 32*(8), 2713–2726. https://doi.org/10.1007/s11095-015-1655-9

Ulvestad, J. S., Kumari, J., Seternes, T., Chi, H., & Dalmo, R. A. (2018). Studies on the effects of LPS, ß-glucan and metabolic inhibitors on the respiratory burst and gene expression in Atlantic salmon macrophages. *Journal of Fish Diseases, 41*(7), 1117–1127. https://doi.org/10.1111/jfd.12806

de Veij, M., Vandenabeele, P., De Beer, T., Remon, J. P., & Moens, L. (2009). Reference database of Raman spectra of pharmaceutical excipients. *Journal of Raman Spectroscopy, 40*(3), 297–307. https://doi.org/10.1002/jrs.2125

Vivcharenko, V., Wojcik, M., & Przekora, A. (2020). Cellular response to vitamin C-enriched chitosan/agarose film with potential application as artificial skin substitute for chronic wound treatment. *Cells, 9*(5). https://doi.org/10.3390/cells9051185

Wang, Q., Xie, J., Zhou, C., & Lai, W. (2022). Substrate stiffness regulates the differentiation profile and functions of osteoclasts via cytoskeletal arrangement. *Cell Proliferation, 55*, Article e13172. https://doi.org/10.1111/cpr.13172

Wessely-Szponder, J., Michalska, J., Szponder, T., Żylińska, B., Tarczyńska, M., & Szubstarski, M. (2020). The role of antimicrobial neutrophil extract in modification of the inflammatory response during osteochondral autograft and allograft transplantation in rabbits. *Journal of Comparative Pathology, 175*, 49–63. https://doi.org/10.1016/j.jcpa.2019.12.007

Wiercigroch, E., Szafraniec, E., Czamara, K., Pacia, M. Z., Majzner, K., Kochan, K. Malek, K., … (2017). Raman and infrared spectroscopy of carbohydrates: A review. *Spectrochimica ActaPart A, Molecular and Biomolecular Spectroscopy, 185*, 317–335. https://doi.org/10.1016/j.saa.2017.05.045

Wojcik, M., Kazimierczak, P., Benko, A., Palka, K., Vivcharenko, V., & Przekora, A. (2021). Superabsorbent curdlan-based foam dressings with typical hydrocolloids properties for highly exuding wound management. *Materials Science and Engineering C, 124*, Article 112068. https://doi.org/10.1016/j.msec.2021.112068

Wojcik, M., Kazimierczak, P., Vivcharenko, V., Koziol, M., & Przekora, A. (2021). Effect of vitamin c/hydrocortisone immobilization within curdlan-based wound dressings on in vitro cellular response in context of the management of chronic and burn wounds. *International Journal of Molecular Sciences, 22*(21), 11474. https://doi.org/10.3390/ijms222111474

Yu, X., Zhang, C., Yang, L., Zhao, L., Lin, C., Liu, Z., & Mao, Z. (2015). CrdR function in a curdlan-producing Agrobacterium sp. ATCC31749 strain. *BMC Microbiology, 15*(1), 25. https://doi.org/10.1186/s12866-015-0356-1

Zdziennicka, J., Szponder, T., & Wessely-Szponder, J. (2021). Application of natural neutrophil products for stimulation of monocyte-derived macrophages obtained before and after osteochondral or bone injury. *Microorganisms, 9*(1), 124. https://doi.org/10.3390/microorganisms9010124

Żelechowska, P., Różalska, S., Wiktorska, M., Brzezińska-Błaszczyk, E., & Agier, J. (2020). Curdlan stimulates tissue mast cells to synthesize pro-inflammatory mediators, generate ROS, and migrate via Dectin-1 receptor. *Cellular Immunology, 351*, Article 104079. https://doi.org/10.1016/j.cellimm.2020.104079

Zhang, R., & Edgar, K. J. (2014). Properties, chemistry, and applications of the bioactive polysaccharide curdlan. *Biomacromolecules, 15*(4), 1079–1096. https://doi.org/10.1021/bm500038g